Comprehensive Study on Melting Process of Phase Change Material by Using Paraffin Coupled Finned Heating Plate for Heat Transfer Enhancement

Lixi Zhang *, Zhengyang Zhang and Hui Yin

School of Power and Energy, Northwestern Polytechnical University, Xi'an 710072, China; villa0913@mail.nwpu.edu.cn (Z.Z.); yhnpu@mail.nwpu.edu.cn (H.Y.)
* Correspondence: zhanglixi@nwpu.edu.cn

Abstract: Paraffin is a low-temperature phase change material, which is often used to recover and store heat in a solar thermal utilization system. This study aims to reveal the development and migration law of paraffin melting interface with time under the influence of a finned heating plate, as well as the heat transfer mechanism, and obtain the ways and methods to enhance the heat transfer in phase change material through visual experiments and numerical simulation. The research shows that once the paraffin with a high liquid fraction connects the mushy zone between the fin and the top wall, the vortexes in the mushy zone increases rapidly, which enhances the natural convective heat transfer in it, resulting in the rapid increase of liquid fraction. The lower the position of the fin, the longer the time required to form a mushy zone with a high liquid fraction between the fin and the top wall, and the later the phenomenon of rapid increase of liquid fraction occurs. Compared with changing the fin position, increasing the fin length has a greater effect on the paraffin melting rate. When other conditions remain unchanged, the inclination of fin and the effective length of fin in the horizontal direction jointly determine the melting rate of paraffin. The melting effect of paraffin is the best when the fin is inclined upward by $15°$.

Keywords: phase change material (PCM); paraffin; fin; melting; visual experiment; heat transfer

1. Introduction

The effective way to reduce carbon emissions and achieve sustainable energy development is to use clean energy and effectively convert and manage energy [1]. Phase change materials (PCM) can store and release a large amount of heat during the phase change process, which can be used to store industrial waste heat, solar energy, and electronic component heat dissipation, and release the stored heat when it is needed [2]. However, the low thermal conductivity of PCM limits its rapid heat absorption and release, which limits its application. In order to improve the thermal conductivity of PCM, many scholars have carried out beneficial innovation and research in different application fields of PCM. Rajvikram et al. [3] used the PCM and the aluminum sheet as the thermal conductivity enhancer to enhance the heat dissipation of the solar photovoltaic panel, reduce the operating temperature of the panel, and improve the power generation efficiency of it.

Studying the phase change heat transfer mechanism of PCM and obtaining the ways and methods to improve the heat transfer rate of PCM is of great significance to expand the application of phase change heat storage. Previously, many researchers have studied the phase transfer process of PCM through numerical simulations and experiments. Eslamnezhad et al. [4] conducted a numerical simulation study on the enhanced heat transfer of PCM melting with rectangular fins, and found that the arrangement of rectangular fins is one of the main factors affecting the melting process. They also proposed the best layout model to improve the efficiency of heat exchangers and to shorten the melting time of PCM. Darzi et al. [5] conducted a numerical study on the melting and solidification processes of

$C_{20}H_{42}$ in three horizontal concentric annular spaces with different diameters. The results showed that the addition of fins can significantly increase the melting and solidification rate. Ji et al. [6] numerically investigated the influence of different fin inclination angles on the melting of lauric acid. Bhagat et al. [7] numerically investigated the influence of fin number, fin thickness and fin height on the temperature of the outlet heat flow in a finned multi-tube latent heat thermal energy storage system. Aly et al. [8] numerically investigated the application of longitudinal corrugated fins in increasing the solidification rate of the formic acid located in the annular area between two concentric tubes. The results show that the effectiveness of the corrugated fins was lower than that of straight fins. Deng et al. [9] investigated the local double-fin at different angles through numerical simulations, of which results compared with the uniform double-fin. Joshi et al. [10] investigated how to obtain the best fin size and fin position to accelerate the melting of the lauric acid. Joybari et al. [11] used a numerical model to investigate the intensity of natural convection for different fins for the inside heating/outside cooling scenario based on the solid–liquid interface evolution over time. Gürel [12] conducted a numerical simulation on the melting heat transfer of the latent heat thermal energy storage system of the plate heat exchanger. Song et al. [13] numerically investigated the melting process of the paraffin outside the finned heating tube, and obtained the movement of the solid–liquid interface with time. By changing the fin thickness, fin pitch and other parameters, the influence of different fin parameters on the melting is analyzed. Biwole et al. [14] numerically investigated the solid–liquid phase change heat transfer in a rectangular enclosure with the aim of optimizing the number, dimension, and positioning of fins in the enclosure. Bondareva et al. [15] numerically investigated heat and mass transfer inside finned heat sink filled with nano-enhanced n-octadecane. Bondareva et al. [16] numerically studied heat transfer inside a domain filled with paraffin with nanoparticles. Masoumpour [17] numerically investigated the melting process of N-eicosane in a storage by inserting innovative fins, which are a combination of rectangular and triangular fins. The impacts of various efficient parameters on melting process are evaluated, which are schematic of internal fins, height of triangular fins, and hot wall temperature. Kim [18] numerically investigated the thermal energy storage performance of a latent heat thermal energy storage system with three angled fins, and the enthalpy-porosity model was used to simulate the phase-change process. To analyze the effect of the angle of inclination of the fin on the heat transfer characteristics and energy storage performance. Wu [19] numerically investigated the comprehensive effect of position and length of the fin in a latent heat thermal energy storage unit with a single fin on the melting and solidification of the lauric acid. The results illustrated that the total melting time was significantly shortened by increasing the fin length and reducing the fin position simultaneously. On the other hand, lowering the fin position would result in non-uniform temperature distribution during the solidification process. Mahood [20] numerically investigated the thermal performance during the melting process for RT-50 in a horizontal latent heat thermal energy storage unit with a view to optimizing the fin configuration. The average temperature of the PCM, its liquid fraction, and velocity distribution during the melting process were investigated. Ghalambaz et al. [21] numerically investigated free convective flow and heat transfer of a suspension of nano encapsulated phase change materials in an enclosure. Singh et al. [22] studied the individual effect of incorporating fins, graphene nano plates, and a combination of both at different volume fractions.

Kamkari et al. [23] used the experimental data to calculate the liquid fraction, the heat transfer rate and Nu during the melting process of lauric acid. The experimental results show that increasing the number of fins can shorten the melting time of PCM and increase the total heat transfer rate, but the surface average Nu decreases. The melting rate and total fin efficiency increase with the increase of the number of fins and the wall temperature. Kamkari et al. [24] studied the influence of the inclination angle of the container on the phase transition of lauric acid with 99% purity. The study showed that the convective flow in the enclosed space increases when the inclination angle decreases from 90° to 0°. When the heating wall temperature is the same, the decrease of inclination angle leads to a

significant increase in heat transfer from one side heated rectangular cavity to PCM. Guo et al. [25] designed and fabricated a complete set of a visual test-bed for the melting front. The results show that the different inclination angle of unit has a great influence on the melting process of pure paraffin. Compared with the inclination of 60°, the total melting time of pure paraffin at the inclination of 30° is reduced by 25.3%. Zheng et al. [26] set up a visual experimental equipment to study the melting process of pure paraffin and foamed copper paraffin (composite phase change material, CPCM). The experiments show that the total melting time of CPCM is 20.5% shorter than that of pure paraffin; the influence of convection on the melting process of CPCM cannot be ignored. Zhang et al. [27] studied the evolution and temperature change of the solid–liquid interface during the melting process. The results show that the temperature distribution of the CPCM composed of paraffin and foamed copper is more uniform than that of pure paraffin, but its natural convection effect is weaker than that of pure paraffin. Ghalambaz et al. [28] used an enthalpy-porosity model to simulate the conjugate flow and heat transfer process of PCM-metal foam in phase change. The results show that heat transfer can be enhanced when heatsink is filled with PCM-metal foam. The results are greatly consistent with experimental studies of the literature works. Yazici et al. [29] experimentally investigated the combined effects of fin number and inclination angle on the thermal performance of a PCM-based heat sink with longitudinal fins. Yagci et al. [30] experimentally investigated the influence of fin shapes with various edge lengths' ratios (upper edge length/lower edge length) on the melting of paraffin with a melting range of 50–58 °C, which is in a vertical annular gap between a heat transfer tube and a shell. Ghalambaz et al. [31] studied the heat transfer and melting flow of PCM under a non-uniform magnetic field. They first utilized the moving grid method to track the interface of phase change. The results show that the magnetic field can greatly affect the melting behavior after the initial period of melting, and the moving grid technique can deal with the phase change heat transfer in the square enclosure well. Sadegh et al. [32] experimentally studied the effects of adding Fe_3O_4 magnetic nanoparticles at various concentrations, as well as applying the magnetic field on the melting process of paraffin as phase change material.

In terms of theoretical research, Diao et al. [33] used the enthalpy porosity technology method to simulate the melting process of PCM, and calculated the liquid fraction according to the enthalpy balance at each iteration, which is the ratio of the liquid zone area occupying the total area of the solid and liquid phases. Bechiri et al. [34] used the separation variable method and the exponential integral function method to solve the transient solid–liquid two-phase energy equation. Ma et al. [35] investigated the flow and heat transfer of micro-encapsulated $C_{18}H_{38}$ based on the Eulerian model. Zhao [36] proposed an improved Nusselt boundary layer model to describe the contact melting process of n-octadecane with 98% purity in a rectangular cavity. Feng et al. [37] proposed a lattice Boltzmann method to solve the solid–liquid phase change coupled with natural convection. Gao et al. [38] proposed an improved lattice Boltzmann method to simulate the natural convection changes of solid–liquid two phases in porous media under local non-thermal equilibrium conditions. Jourabian et al. [39] used the lattice Boltzmann method to study the melting phenomenon with natural convection in a square cavity with a fin. Zhang et al. [40] reviewed the research on enhancing the heat transfer performance of phase change materials using microcapsules, metal materials, carbon materials and heat pipe technologies, and analyzed and summarized the advantages and disadvantages of various methods for enhancing heat transfer of phase change materials. Zhu [41] used experimental methods to study the heat transfer process of constrained melting and unconfined melting under isothermal heating conditions.

In this paper, using paraffin as PCM, the development and migration of paraffin melting interface with time when heating paraffin are studied by means of visual experiment and numerical simulation. Additionally, the effects of fin position, length and inclination on the liquid fraction and micro flow state in the mushy zone when a fin is added to the

heating plate are simulated and analyzed, in order to provide a method and basis for strengthening phase change heat transfer.

2. Visual Experiments

2.1. Visual Experiments

A visual experimental system for the heating and melting process of PCM was established as shown in Figure 1. The development and migration law of PCM melting interface with time were observed. Several K-type thermocouples were used to monitor the temperature change inside the paraffin. The influence of different heating power on the phase change melting process was studied.
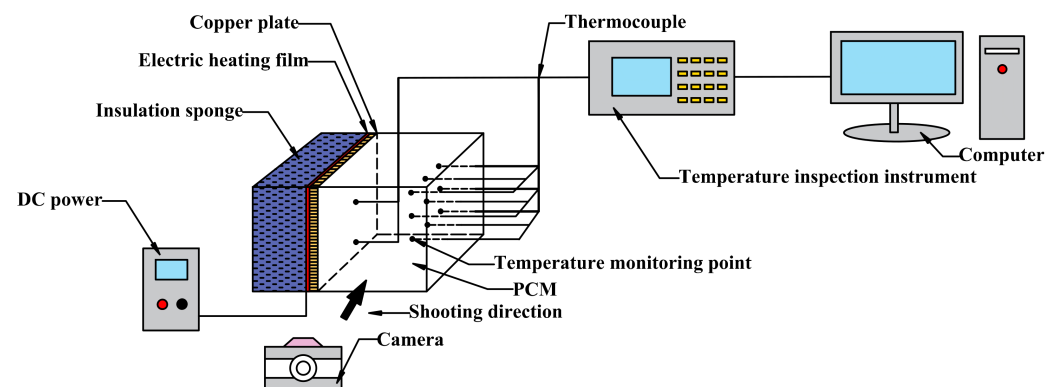

Figure 1. Schematic diagram of visual experimental system for phase change material (PCM) melting process.

The location and the number of the thermocouples are shown in Figure 2. The heating power is 20 W, and the outer surface of the test piece is insulated with an insulation sponge.
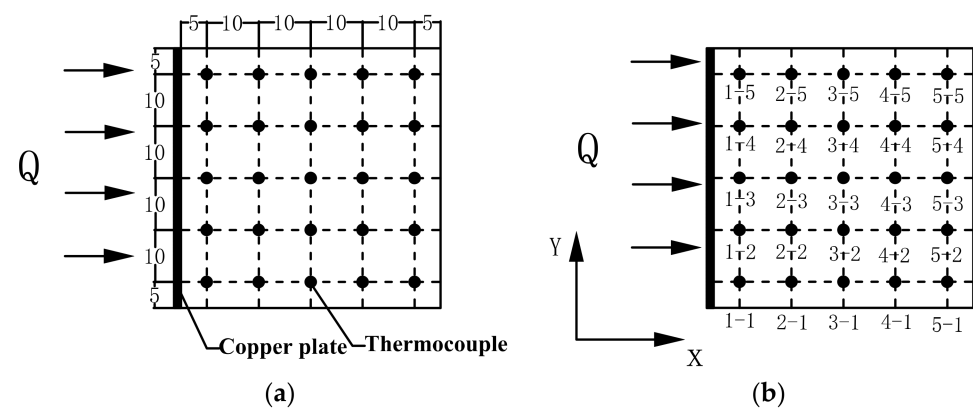

Figure 2. Schematic diagram of position and number of thermocouples. (**a**) Schematic diagram of thermocouple arrangement spacing (unit: mm); (**b**) schematic diagram of thermocouple number.

In the experiment, two 25 mm × 50 mm electric heating films are connected in series as a heater. DC power is used to adjust the output thermal power of the heater by adjusting the voltage of the DC power supply. In order to meet the boundary heating conditions of equal heat flux density, with the help of the high thermal conductivity of copper, first we heated the 0.5 mm copper plate with a heater, and then heated the paraffin on its right side with the copper plate. The electric heating power can be obtained by measuring the voltage and current of the heater, and then the heating power can be divided by the area of the copper plate to obtain the heat flux density of the copper plate.

The fin and the copper plate are made of the same material, and their physical parameters are from the Fluent database, as shown in Table 1.

Table 1. Physical parameters of copper plate and fin materials.

Density kg/m^3	Thermal Conductivity W/(m·K)	Specific Heat kJ/(kg·K)
8978	387.6	381

2.2. Physical Properties of Paraffin

The PCM used in the experiments is paraffin with the phase change temperatures of 48–50 °C, and its physical parameters are shown in Table 2.

Table 2. Physical parameters of paraffin [2,42].

Phase	Phase Change Temperature K	Density kg/m^3	Thermal Conductivity W/(m·K)	Specific Heat kJ/(kg·K)	Latent Heat of Fusion kJ/kg	Dynamic Viscosity kg/(m·s)
Solid	321	912	0.295	2.40	189	-
Liquid	323	769	0.118	1.89	-	0.0029

3. Numerical Simulation of Phase Transition Process

3.1. Basic Equations of the Numerical Simulation

The enthalpy-porosity method is a based on the numerical value of enthalpy to solve the problem of phase change. This method converts the temperature variable in the control equation into the enthalpy variable, and determines the two-phase distribution by solving the enthalpy value in the whole region. Its calculation process is relatively simple. In this method, the mushy zone is regarded as a porous area, and its porosity is equal to the liquid fraction. Here, the enthalpy-porosity method is used to calculate the solid–liquid phase change heat transfer.

In the process of solid–liquid phase transition, because the position of the mushy zone moves with time, the transient governing equations are used to simulate the transient melting process of PCM. Considering the influence of the natural convection of the PCM in the heat transfer process, the basic equations of the numerical simulation are [43]:

1. Mass conservation equation

$$\nabla \cdot U = 0 \tag{1}$$

Here, U—the velocity vector of PCM, m/s.

2. Momentum conservation equation

The enthalpy-porosity method regards the mushy zone as a porous medium, and the porosity in each grid is equal to its liquid fraction f. In the solid region, the porosity is zero. There is a source item in the momentum equation that makes the porosity affect the velocity. The momentum equation is as follows [40]:

$$\rho \frac{\partial U}{\partial t} + \nabla \cdot (\rho U U) = \nabla \cdot (\rho v \cdot \nabla U) - \nabla F + S_m \tag{2}$$

In the above formula, ρ—density, kg/m^3; t—time, s; v—the kinematic viscosity of the material, m^2/s; and F—pressure, Pa·S_m is the source term of the momentum equation; it makes the porosity change act on the fluid velocity, even if the fluid velocity in the mushy zone varies with porosity. The porosity in each grid is equal to its liquid fraction f in the enthalpy-porosity method, so S_m can be expressed as [41]:

$$S_m = \frac{(1-f)^2}{(f^3 + \varepsilon)} A_{mush} U + \frac{\rho_0 g f (h - h_0)}{c_p} \tag{3}$$

Here, f—liquid fraction; ε—a small computational constant used to avoid division by zero (normally it is taken a number less 0.001); ρ_0—density at T_0, kg/m^3; A_{mush}—constant of mushy zone, generally it is (10^4~10^7) kg/(m^3·s) [44]. However, Shmueli et al. [45] concluded by comparing with the experiment that when A_{mush} takes 10^8 kg/(m^3·s), it is more accurate for the simulation of the paraffin melting process.

3.　Energy conservation equation

The PCM can be calculated using its sensible enthalpy h_s and latent heat Δh [40]:

$$h = h_s + \Delta h \tag{4}$$

h_s can be expressed as [40]:

$$h_s = h_0 + \int_{T_0}^{T} c_p dT \tag{5}$$

Here, h_0—enthalpy in reference state, kJ/kg; T_0—temperature in reference state, K; c_p—constant-pressure specific heat, kJ/(kg·K).

Δh can be expressed as [40]:

$$\Delta h = fQ \tag{6}$$

Here, Q—latent heat of phase change, kJ/kg.

The energy conservation equation can be written as [40]:

$$\frac{\partial}{\partial t}(\rho h) + \nabla \cdot (\rho U h) = \nabla \cdot (k \nabla T) + S_e \tag{7}$$

In the formula, U—fluid velocity, m/s; S_e—heat flow source term of the energy equation, and it can be expressed as [40]:

$$S_e = \frac{\rho}{c_p} \frac{\partial(\Delta h)}{\partial t} \tag{8}$$

The solidification and melting model are used to simulate the phase change heat transfer process, which is based on the enthalpy-porosity method to solve the phase change process. The mushy zone is regarded as the porous medium zone. Liquid fraction (porosity) is defined as [40]:

$$\begin{cases} f = 0 \ T < T_s \\ f = 1 \ T > T_s \\ f = \frac{T - T_s}{T_l - T_s} \ T_s < T < T_l \end{cases} \tag{9}$$

T_s—solidification temperature of PCM, K; T_l—melting temperature of PCM, K.

The region where f is between 0 and 1 is a mushy zone, in which the substance is a solid-liquid mixture. When $f = 1$, the PCM is completely melted into a liquid; when $f = 0$, the PCM is completely solidified into a solid.

4.　Energy equation for fin

In Figure 1, for the paraffin in the container, the copper plate is a heating plate. When a heat transfer fin is installed on the heating plate, the geometry of the fin is shown in Figure 3. The wall in the figure is the heating plate.
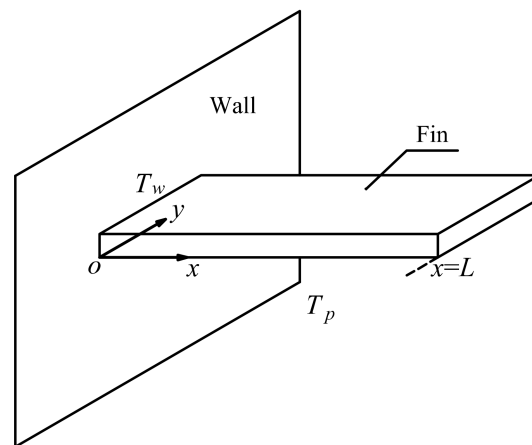
Figure 3. Geometry of the heat transfer fin.

where L—the length of fin, m; T_w—the temperature of wall, K; T_p—the temperature of paraffin near the fin, K. Assuming the temperature within the fin is a function of x only, $T = T(x)$.

Because the paraffin in contact with the surface of the fin will melt soon after the heating starts, the heat transfer mode between the surface of the fin and the paraffin is considered as convective heat transfer, while the heat transfer mode inside the fin is heat conduction. For a micro volume element Adx in the fin, the energy balance of it is shown in Figure 4.
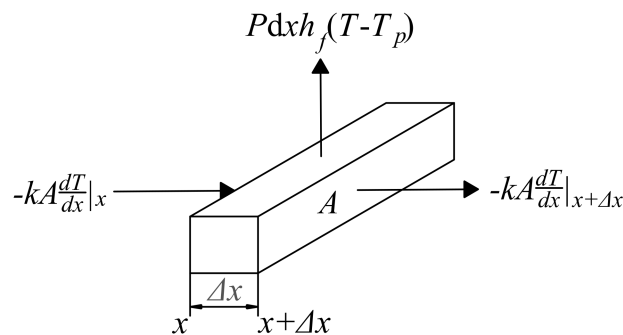
Figure 4. Schematic diagram of energy balance in fin micro element.

The energy balance relationship of the fin micro element is

$$-kA\left.\frac{dT}{dx}\right|_x = Pdxh_f(T - T_p) - kA\left.\frac{dT}{dx}\right|_{x+\Delta x} \tag{10}$$

Here, k—the thermal conductivity of copper fin, W/ (m·K); A—the cross-section of fin, m^2; P—the perimeter of fin, m; Pdx—the heat transfer area between fin micro element and paraffin, m^2; h_f—the heat transfer coefficient between fin and paraffin, W/(m^2·K).

Using second-order Taylor series expansion, it is possible to obtain:

$$-kA\left.\frac{dT}{dx}\right|_{x+\Delta x} = -kA\frac{dT}{dx} - kA\frac{d^2T}{dx^2}dx \tag{11}$$

Combining Equations (10) and (11), the energy balance equation of fin micro element can be expressed as:

$$\frac{d^2T}{dx^2} - \frac{Ph_f}{kA}(T - T_p) = 0 \tag{12}$$

Because the left end of the fin joins the wall, so the boundary condition at $x = 0$ is:

$$x = 0, \ T = T_w \tag{13}$$

At the other end of fin, assuming the heat transfer from this end is negligible, the boundary condition is:

$$x = L, \ \frac{d}{dx}(T - T_p)\big|_{x=L} = 0 \tag{14}$$

3.2. Simplified Geometric Model for Numerical Simulation

In the experimental system, the size of the paraffin container is 50 mm $\times$ 50 mm $\times$ 50 mm, and it is heated only by the left side heating copper plate.

For the paraffin melting process, the transient numerical simulation is needed. If the three-dimensional model is adopted, the calculation time will be long, and the simulated calculation is difficult to converge. However, the two-dimensional model can not only better show the melting process, but is also easy to converge. Therefore, according to the symmetry of the paraffin container, a two-dimensional model and the structured meshes are used in numerical simulation, and the size of geometric model for numerical simulation is the same as that of the experiment, as shown in Figure 5.
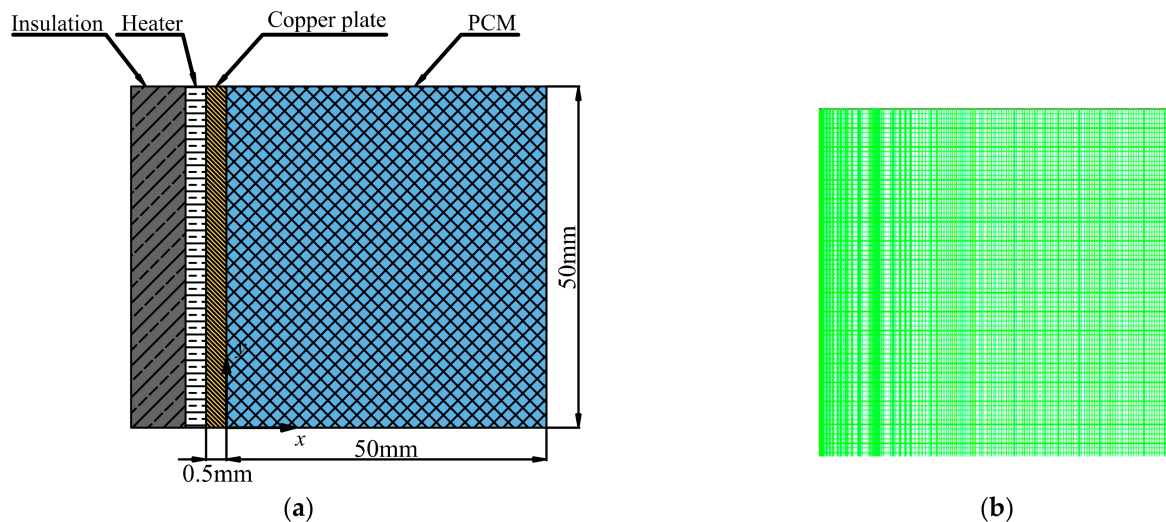

Figure 5. Geometric model and its structured meshes. (**a**) Geometric model; (**b**) structured meshes of the model.

3.3. Numerical Method and Boundary Conditions

For the Figure 5a, the Fluent software is employed to do the numerical simulation for the PCM melting process. The energy equation needs to be opened, and the solidification and melting model is adopted. The first-order upwind discrete scheme and SIMPLE algorithm are used. The PRESTO! scheme is selected for porous media. The influence of gravity is considered, and the gravity acceleration is taken as -9.81 m/s^2 in the vertical direction. New paraffin material attribute settings need to be created, and the cell zone conditions are set to paraffin and the copper plate area set to solid copper. The relaxation factors and other parameters are set by default. The time step is set to 0.5 s, the maximum number of iterations of each step is set to 40, and the number of time steps is set to 1800; that is, the actual duration of simulation is 900 s. For the variable parameter C of the PCM mushy zone, here C is A_{mush} of Equation (3), and the value 10^8 recommended by Shmueli et al. [45] for paraffin is adopted. The convergence criterion is set as 10^{-4} for the continuity equation and the velocity equation, and 10^{-6} for the energy equation.

The two-dimensional heat conduction equation for solid paraffin is [46]:

$$k_p\left(\frac{\partial^2 T}{\partial x^2} + \frac{\partial^2 T}{\partial y^2}\right) = \rho c_p \frac{\partial T}{\partial t} \tag{15}$$

where k_p—the thermal conductivity of paraffin, W/(m·K).

In the setting of boundary conditions, the junction of copper plate and paraffin is set as coupled boundary conditions. The growth rate of the boundary layer in the simulation is 1.2. For the Figure 5a, at the junction of the left copper wall and PCM, the boundary conditions are the continuities of temperature and heat flow, shown as follows [47]:

$$T_w\big|_{x=0} = T_p\big|_{x=0} \tag{16}$$

$$q = -k\frac{\partial T}{\partial x}\bigg|_{x=0} = -k_p\frac{\partial T}{\partial x}\bigg|_{x=0} \tag{17}$$

where, T_w—the temperature of wall, K; T_p—the temperature of paraffin, K; q—the heat flux supplied by heating plate, W/m^2; k_c—the thermal conductivity of copper, W/(m·K). In the simulation, the value of q is taken as 8000 W/m^2.

Except the left wall, the other walls of the paraffin container are treated with the third kind of boundary conditions. The boundary conditions are:

$$-k_p\frac{\partial T}{\partial y}\bigg|_{y=b} = h_a(T_w - T_f) \tag{18}$$

$$-k_p\frac{\partial T}{\partial y}\bigg|_{y=0} = h_a(T_w - T_f) \tag{19}$$

$$-k_p\frac{\partial T}{\partial x}\bigg|_{x=a} = h_a(T_w - T_f) \tag{20}$$

Here, a—the length of PCM container, mm; b—the height of PCM container, mm; h_a—the natural convection heat transfer coefficient between the wall and air, W/(m^2·K); T_f—the temperature of air, K. Since the experiment is carried out indoors, in order to make the numerical simulation conditions closer to the experimental conditions, the value of h_a is taken as 3 W/(m^2·K) in the simulation.

Figure 6 is the comparison of the liquid fraction under three different mesh numbers. Under the condition that the heating power is 20 W, the heat flux density is 8000 W/m^2; the initial temperature of the paraffin is 303 K. When the number of meshes is 0.10 million, 0.15 million and 0.18 million, respectively, the liquid fraction at the end of the simulation is, respectively, 31.6%, 31.8% and 32.0%. This means that the liquid fraction under different numbers of meshes has little difference. The largest error during the simulation is 1.25%. Therefore, the number of meshes for the simulation is taken as 0.15 million.

3.4. Comparisons between Numerical Simulation Results and Experimental Results

When the heating power is 20 W, the comparison of the experiment and the numerical simulation results of the paraffin melting process at different times is shown in Figure 7, and the comparison of the experimental temperatures and the simulated ones at the internal monitoring points of paraffin is shown in Figure 8.

It can be seen from the two figures that the experimental and numerical simulation results are basically the same, indicating that the numerical simulation method is correct. In Figure 7, the melting interface change of the experiment is slightly slower than that of the numerical simulation. On the one hand, there is heat loss to the environment in the experiment; on the other hand, there is an error in the numerical simulation itself. They both cause the difference between the numerical simulation and the experiment.
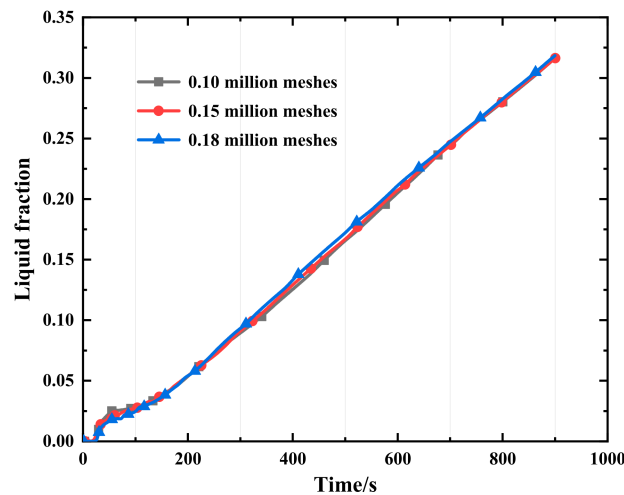
Figure 6. Comparison of liquid fraction under three different mesh numbers.

Figure 8 is the comparison of experimental temperatures and simulated temperatures at internal monitoring points of paraffin. The locations of these monitoring points are shown in Figure 2b. It can be seen from the Figure 8 that the experimental results are basically consistent with the simulation results.
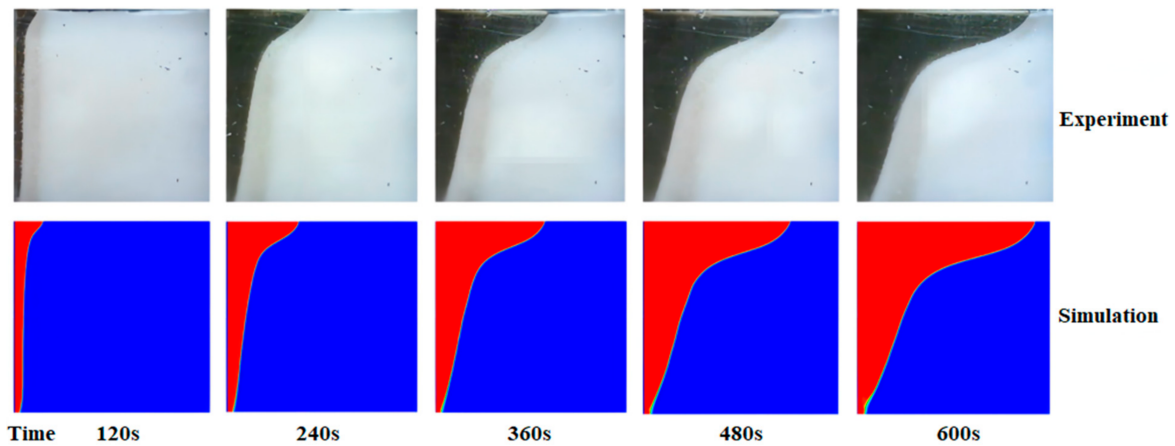

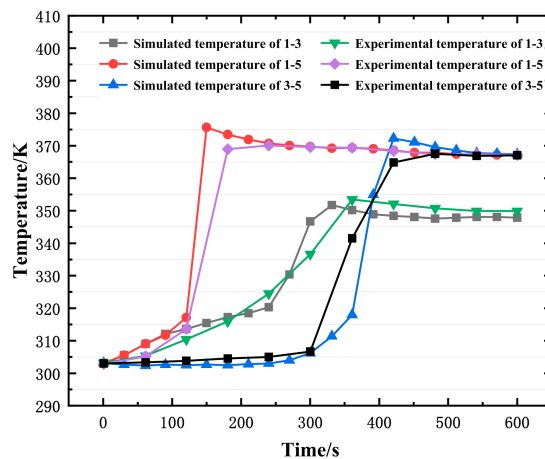**Figure 7.** Comparison of experimental and simulated results of paraffin melting process at different times.

Figure 8. Comparison of experimental temperatures and simulated temperatures at internal monitoring points of paraffin.

4. Numerical Simulation of Influencing Factors of Phase Transition Process

In the numerical simulation, in order to reduce the number of the meshes and the time of calculation, the width of the simulation model is only taken as the half width of the experimental model, which is rectangular as shown in Figure 9. The model is filled with paraffin and heated only by the left side wall.
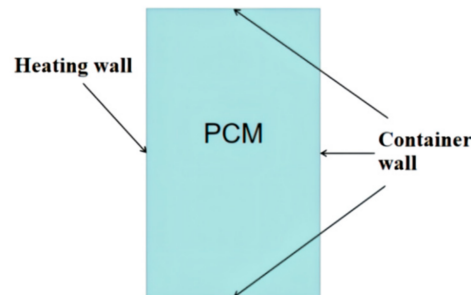

Figure 9. Geometric model of numerical simulation.

4.1. Influence of Time

Figure 10 is the contours of solid–liquid interface of the PCM at different moments. The top of the PCM container is the adiabatic wall. It can be seen from the Figure 10 that the PCM melts unevenly at the vertical direction. At the higher part of the container, the PCM melts more than that at the lower part; this is because the liquid phase has lower density, resulting in the upward flow of the liquid phase with higher temperature, bringing heat to the higher part. Finally, the melting amount in the higher position area is increased.
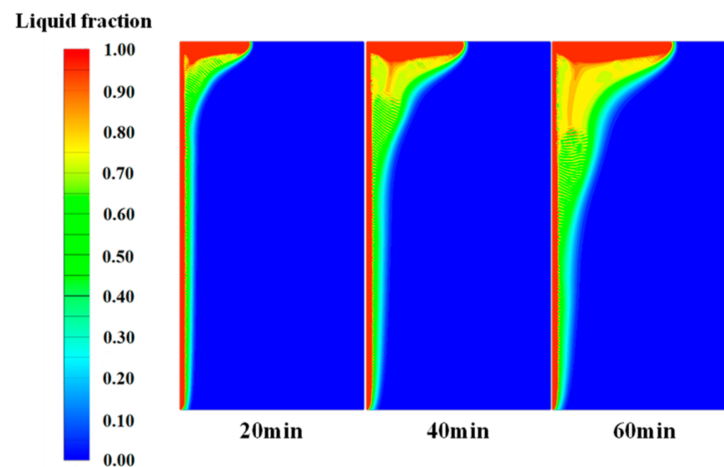

Figure 10. Contours of solid–liquid interface at different times.

4.2. Influence of Fin

As shown in Figure 5, in order to realize uniform heating on the left side of the PCM container in the experiment, the heated copper plate is used, and its thickness is only 0.5 mm. If a fin is welded on the thin copper plate, the general processing level cannot ensure the flatness of the welded joint, and the unevenness caused by welding may affect the flow and heat transfer in the experiment. Therefore, when the container has a fin, the numerical simulation method is used to study it.

Figure 11 is a geometric model with a fin on the heating wall. The fin is made of copper, its length is $L = 10$ mm, thickness is $\delta = 0.5$ mm, and height is $H = 24.75$ mm.
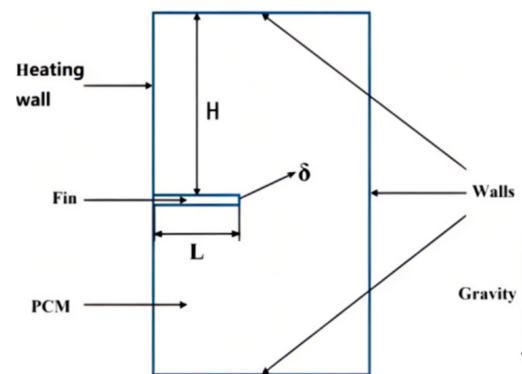
Figure 11. Numerical simulation geometric model of a heating wall with a fin.

Because the fin is very thin, in the simulation calculation, the number of grids and the time spent when using a fin are not much more than that without using a fin.

Figure 12 is the contours of solid–liquid interface with and without a fin at different times. In each cloud chart below, *f* represents the liquid fraction, which increases with heating time under the same other conditions. After heating for 60 min, the liquid fraction of paraffin with a fin on the heating plate is up to 0.272, which is almost two times that of without a fin. The larger the liquid fraction, the greater the heat storage capacity of the PCM. Because the actual heat storage capacity of PCM is equal to the product of the liquid fraction, total volume of PCM and phase change latent heat.

It can be seen from Figure 12 that due to the existence of fin, the heat transfer and the melting of paraffin are accelerated, and the vortex velocity field appears near the fin.

Figure 13 is the streamline diagrams around the fin of paraffin at different times. It can be seen from the figure that at the initial stage of heating, the paraffin near the heating wall melts first and the liquefied paraffin flows upward; when the hot fluid reaches near the top wall of the container, it turns the flow direction and starts to flow downward, forming vortexes under the top wall and near the heating wall; When the fluid continues to flow down to the upper surface of the fin, it flows to the right again, and finally converges with the fluid from the lower surface of the fin to form a vortex again; at the same time, the liquefied paraffin under the fin forms vortexes between the heating wall and the fins.
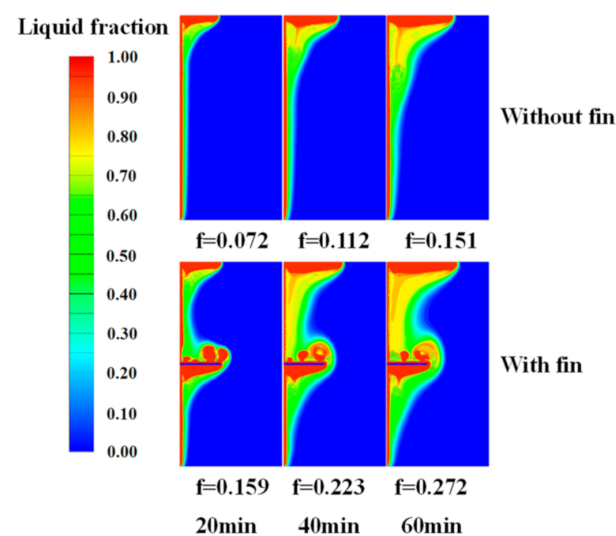

Figure 12. Contours of the solid–liquid interface with and without a fin at different times.
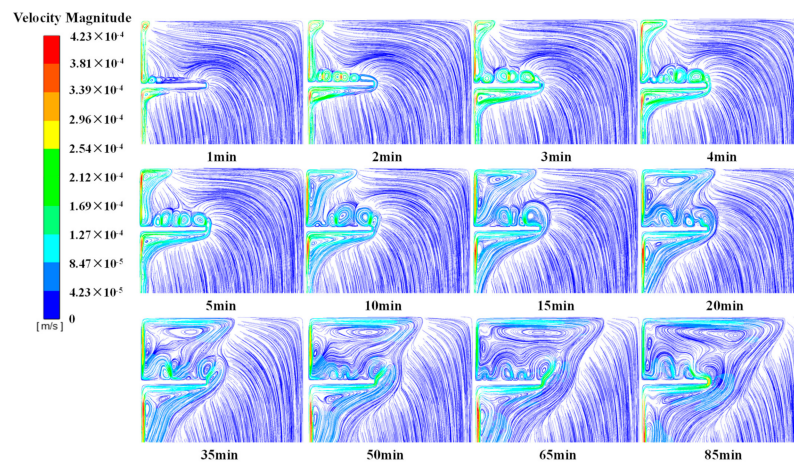
Figure 13. Streamlines around the fin in paraffin at different times.

These vortexes enhance the fluid disturbance and natural convection heat transfer in the paraffin mushy zone, accelerating the melting of paraffin and the expansion of the mushy zone.

Figure 14 is the temporal variation of liquid fraction with and without a fin. It can be seen that the melting rate of paraffin with fin on the heating plate is nearly 70% faster than that without fin on the heating plate.
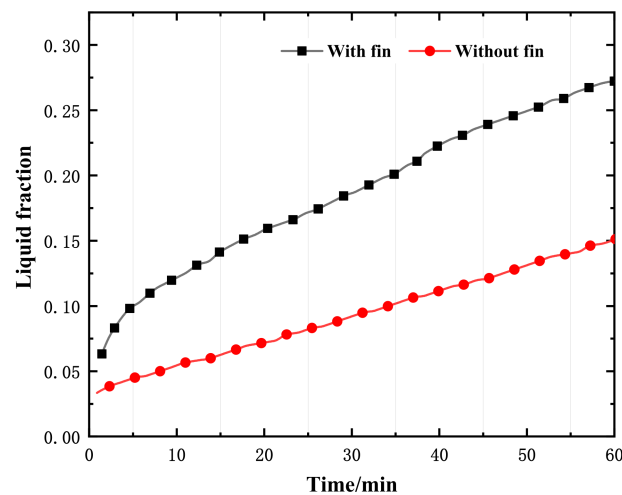

Figure 14. Temporal variation of liquid fraction with and without a fin.

4.3. Influence of Fin Position

Under the influence of gravity and natural convection, the PCM melts unevenly at the vertical direction, so the position of the fin on the wall will affect the melting process. The distance between the top surface of the fin and the top wall of the container is defined as *H*, and *H* is taken as 9.75, 19.75, 29.75 and 39.75 mm, respectively.

Figure 15 is the contours of the solid–liquid interface and liquid fractions of the PCM at different fin positions and different heating time.

Figure 16 shows the temporal variation of the liquid fraction with different fin positions *H*. It can be seen from Figures 15 and 16, as the heating time increases, the increasing rate of liquid fraction gradually decreases. In the first 15 min, when *H* is 9.75 mm, the melting rate is the fastest; at the heating time between 20 min and 50 min, when *H* is 19.75 mm, the liquid fraction is the largest; at the heating time between 53 min and 80 min, when *H* is 29.75 mm, the liquid fraction is the largest; at the heating time between 60 min and 90 min, when *H* is 9.75 mm, the liquid fraction is the smallest.
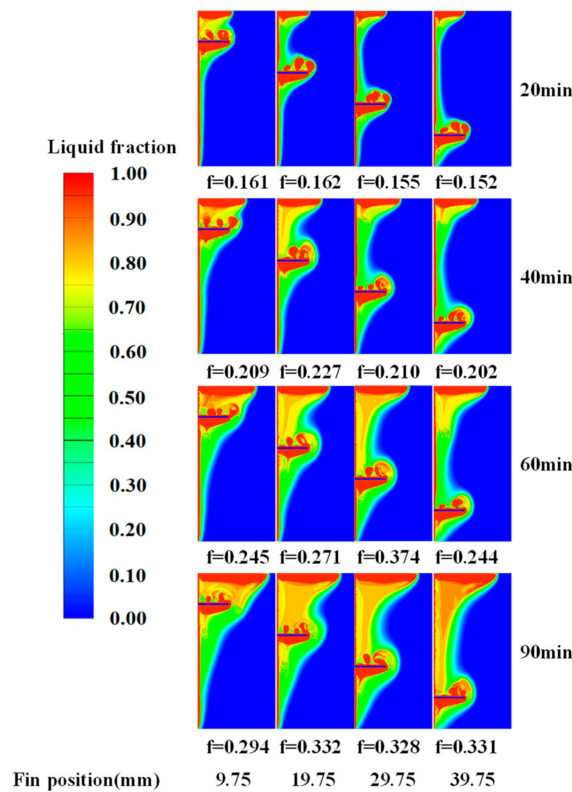
Figure 15. Contours of the solid–liquid interface and liquid fractions at different fin positions.

In Figure 16, when *H* is 19.75, 29.75 and 39.75 mm, respectively, the liquid fraction suddenly increases at about 28, 50 and 74 min, respectively. That is, the larger the *H*, the later the sudden increase of liquid fraction *f* occurs. Before the sudden increase of *f*, due to the continuous upward flow of liquid paraffin, it mainly expands outward along the horizontal direction after reaching the top wall.

The greater the *H*, the further the fin is from the top wall, and the longer the time required to form a mushy zone with a high liquid fraction between the fin and the top wall. Once the mushy zone with high liquid fraction is formed, the larger the area of natural convection, the stronger the natural convection heat transfer, and the faster the melting rate of paraffin. When *H* = 9.75 mm, it can be seen from Figure 16 that there is no sudden increase of *f*. Under this condition, the fin is close to the top wall, and the mushy zone with a high liquid fraction is formed quickly, which is why the melting rate is the fastest compared with other *H* values in the first 15 min of heating.
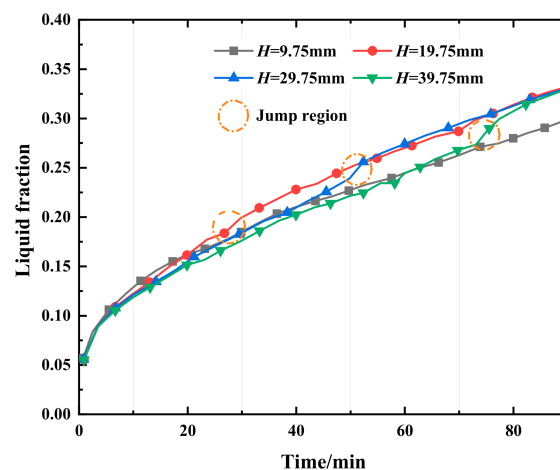

Figure 16. Variation of paraffin liquid fraction with time under different fin positions.

Figure 17 is the corresponding contours of the solid–liquid interface around three jump points of *f* at 28 min, 50 min and 74 min, when *H* is 19.75 mm, 29.75 mm and 39.75 mm, respectively. Within two minutes, the liquid fraction in the mushy zone increases sharply from 0.6 to about 0.85. Near the time points above, the paraffin area with high liquid fraction continues to expand from top to bottom until it connects with the paraffin with a high liquid fraction of about 0.95 near the fin. The connectivity of paraffin with the high liquid fraction in the mushy zone leads to the enhancement of natural convection heat transfer in the mushy zone, which leads to the obvious increase of *f*.

The streamlines corresponding to the paraffin at the time near the three jumps in Figure 16 are shown in Figure 18. It can be seen from Figure 16, in the mushy zone, that vortexes near the heating wall increase rapidly during this period, and the flow becomes more complex, and the natural convection is enhanced, resulting in a sudden increase of the melting rate of paraffin.
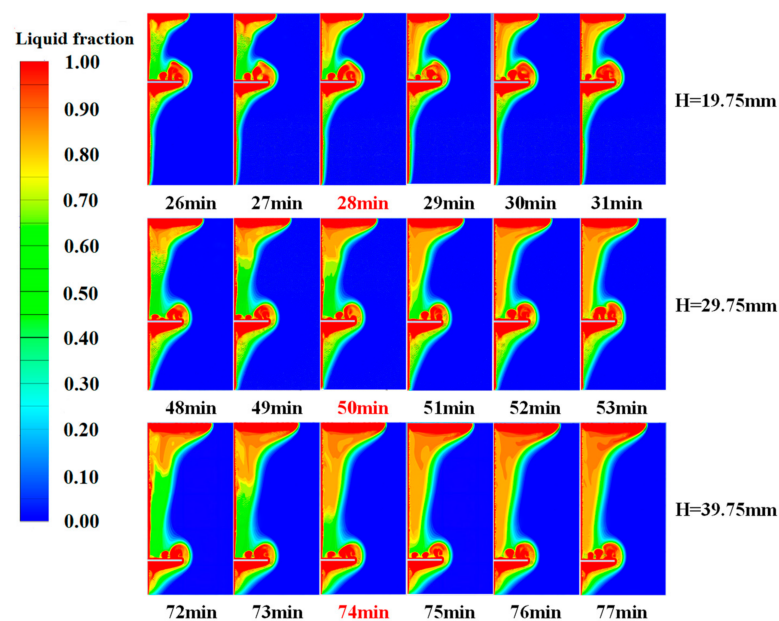

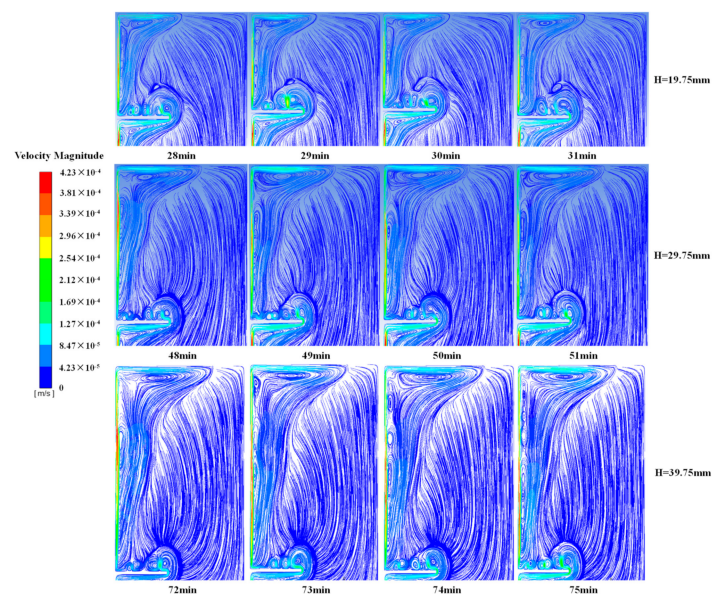**Figure 17.** Contours of the solids-liquid interface around three jump points of *f*.

Figure 18. Streamlines of paraffin around three jump points.

4.4. Influence of Fin Length

When *H* is 24.75 mm, the fin is in the middle position of the heating wall. In this case, the fin length *L* is taken as 5, 10, 15 and 20 mm respectively for the numerical simulation calculation.

Figure 19 shows the contours of the solid–liquid interface and liquid fraction under different fin lengths, and Figure 20 shows the variation of liquid fraction with time under different fin lengths. It can be seen from the figures that the liquid fraction increases with the increase of the fin length under each working condition. This is because, with the increase of fin length, the contact area between fin and PCM increases, thus accelerating the melting of PCM. Compared with changing the fin position, increasing the fin length has a greater effect on the melting rate of paraffin.
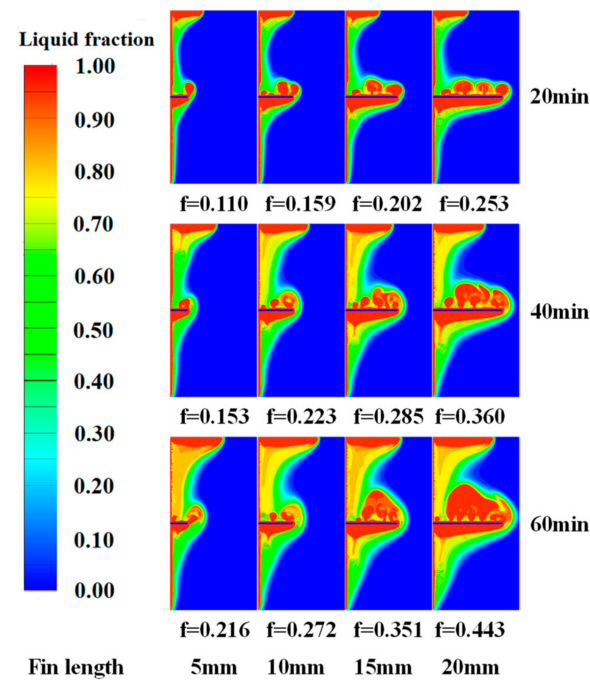

Figure 19. Contours of the solid–liquid interface and liquid fraction under different fin lengths.
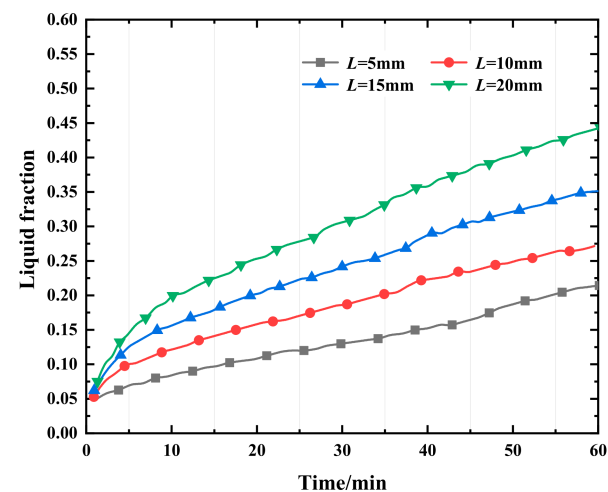

Figure 20. Variation of liquid fraction with time under different fin lengths.

4.5. Influence of Fin Inclination

When the fin is in the center of the container wall, the distance of which to the top wall is 24.75 mm, the length of fin is 10 mm. The fin can be inclined upward or downward, and

the angle α between fin and horizontal plane is 0°, 15°, 30°, 45°, 60° and 75°, respectively. It is assumed that when the fin is installed at different angles, the shape of the fins is the same, but the installation angles are different.

Figures 21 and 22 show the contours of the solid–liquid interface of the PCM at different moments and with different fin inclined angles. In Figure 21, it is obvious that when the fin is inclined upwards by 15°, the liquid fraction at 60 min is the largest, being 0.282. When the fin is inclined upwards, as the angle increases, the melted PCM below the fin flows upwards more easily, accelerating the melting of the PCM at the higher part; however, at the same time, the effective length of the fin in the horizontal direction will decrease, slowing down the melting of the PCM. These two factors jointly restrict the melting rate of the PCM.
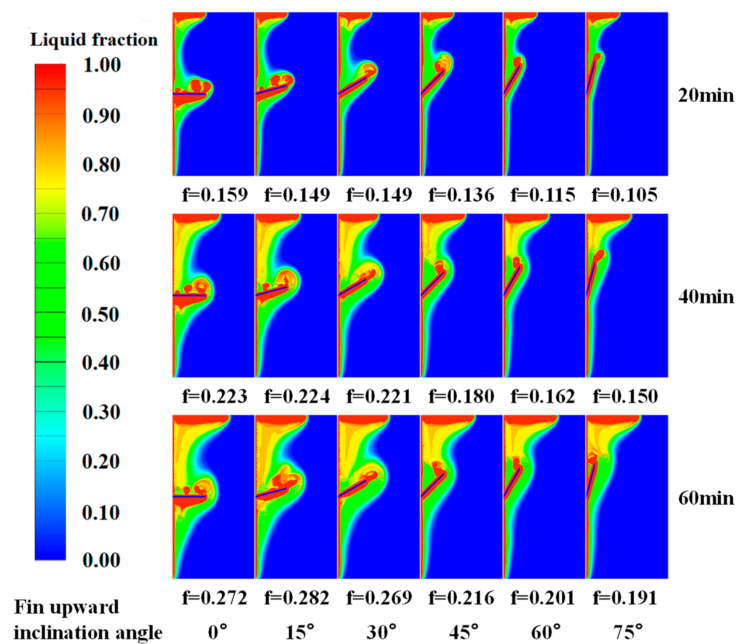

Figure 21. Contours of the solid–liquid interface and liquid fraction with the fin inclined upward at different angles.
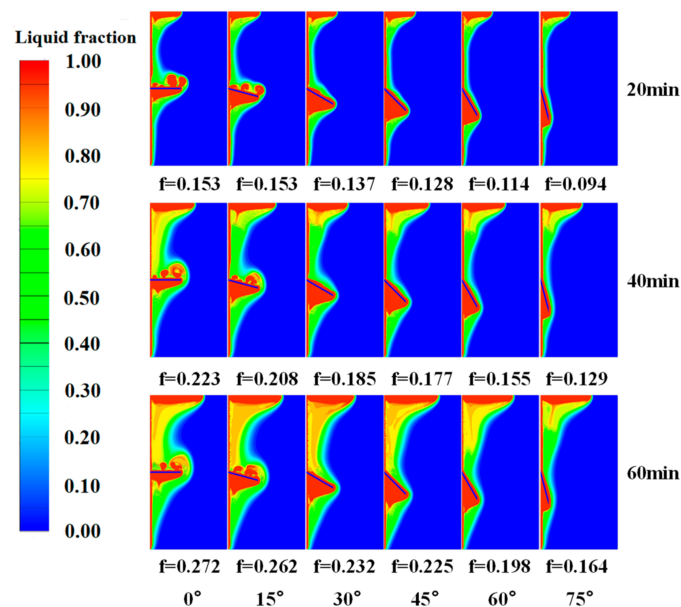

Figure 22. Contours of the solid–liquid interface and liquid fraction with the fin inclined downward at different angles.

When the fin is inclined downwards, as the heating time increases, the liquid fraction is always smaller than that when the fin is arranged horizontally ($\alpha = 0°$), which means that the downward inclination of the fin is not conducive to the heat exchange and melting of the PCM. This is because the melted PCM below the fin is resisted by the fin and it is difficult for it to flow upward. At the same time, the effective length of the fin in the horizontal direction decreases due to the inclination of the fin. These two factors lead to the reduction of the melting rate of PCM.

Figure 23 shows the streamlines of paraffin at different times when the fin is inclined upward 15° and downward 15°, respectively. It can be seen from Figure 21, compared with the fin inclined downward by 15°, when the fin is inclined upward by 15°, the melted paraffin flows upward more easily and the vortex on the upper surface of the fin is larger. Combined with Figures 21 and 22, when the fin is inclined upward by 15°, the natural convection and heat transfer in the melted paraffin above the fin are stronger and the liquid fraction is larger.
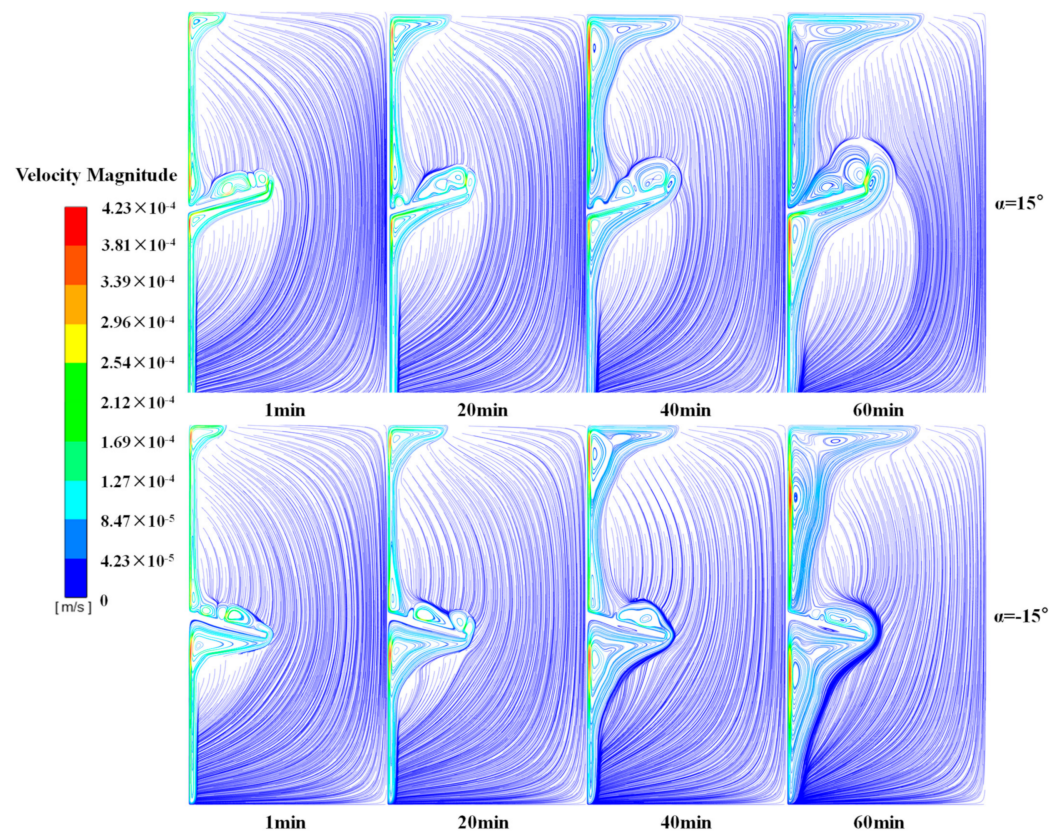

Figure 23. Streamlines of paraffin under different fin inclined angles at different times.

Figures 24 and 25 show the relationship between the liquid fraction and time when the fin is inclined upward and downward from 0° to 75°, respectively. It can be seen from Figures 21 and 24 that the melting effect is the best when the fin is inclined upward by 15°. This is because the fin is properly inclined upwards, which helps the melted PCM below the fin to flow upwards more easily, and helps the natural convection heat transfer in the liquid phase to accelerate the melting of the PCM above the fin; at the same time, the fin length in the horizontal direction is not significantly reduced. In the reference [6], when the double-fins are inclined downward by 15°, the melting effect of a commercial PCM, RT42, is the best, which means that interference between each fin effects the flow characteristics and heat transfer in the melting process.
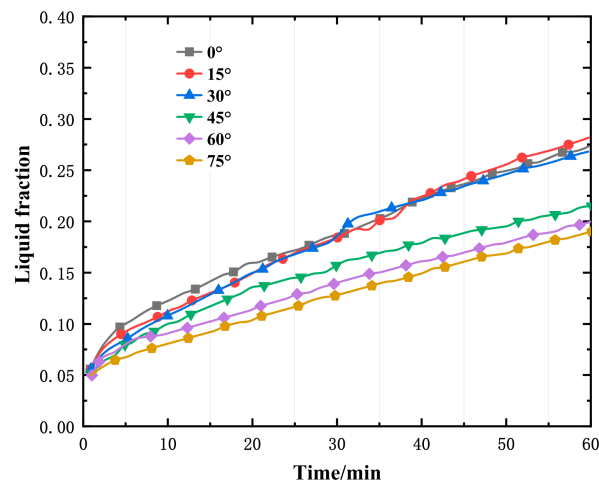
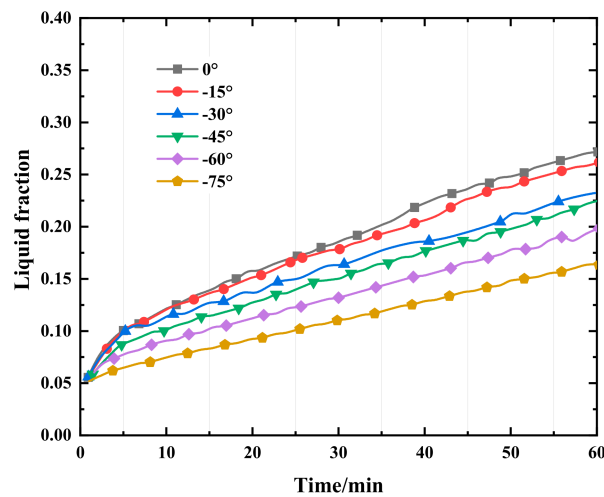**Figure 24.** Temporal variation of liquid fraction with the fin inclined upward.

Figure 25. Temporal variation of liquid fraction with the fin inclined downward.

5. Conclusions

In this study, the development and migration law of the paraffin melting interface with time are revealed by visual experiment and numerical simulation; When installing fin on the heating plate, the heating and melting process of paraffin under different fin positions, fin lengths and fin inclination angles are simulated and compared. The research conclusions are as follows:

1. After adding a fin to the heating plate, the mushy zone becomes larger obviously. A vortex velocity field is formed near the fin, which strengthens the natural convective heat transfer and accelerates the melting of paraffin.

2. Once the mushy zone between the fin and the top wall is connected by paraffin with a liquid fraction greater than 80%, the vortex in the mushy zone will increase, resulting in the enhancement of natural convection heat transfer and the rapid increase of the liquid fraction; that is, the melting of paraffin will accelerate.

3. The lower the position of the fin, the longer the time required to form a mushy zone with a high liquid fraction between the fin and the top wall, and the later the phenomenon of rapid increase of liquid fraction occurs; the longer the fin, the larger the contact area between the fin and paraffin. The effect of fin length on paraffin melting rate is greater than that of fin position.

4. When the fin is inclined upward, the paraffin melted under the fin will more easily flow upwards, thus accelerating the melting of paraffin above the fin. At the same time, the effective length and heat transfer of the fin in the horizontal direction are

reduced. The two factors together determine the melting rate of paraffin. It is shown that when the fin is inclined upward by 15°, the melting effect of paraffin is the best.

The research conclusions of this paper have reference value for the application of paraffin in solar thermal utilization system and other related fields.

Nomenclature

a	length of PCM container, mm	L	fin length, mm
A	cross-section of fin, m^2	Q	latent heat of phase change, kW
A_{mush}	constant of mushy zone, kg/(m^3·s)	P	perimeter of fin, m
b	height of PCM container, mm	P_{dx}	heat transfer area between fin micro element and paraffin, m^2
c_p	constant-pressure specific heat, kJ/(kg·K)	q	heat flux, W/m^2
f	liquid fraction	t	time, s
F	pressure, Pa	T_f	temperature of air flow, K
h	enthalpy, kJ/kg	T_l	melting temperature, K
H	distance between the upper surface of fin and the top wall of container, mm	T_p	temperature of paraffin, K
h_{a}	natural convection heat transfer coefficient between wall and air, W/(m^2·K)	T_w	temperature of wall, K
h_f	heat transfer coefficient between fin and paraffin, W/(m^2·K)	T_{o}	temperature in reference state, K
h_{s}	sensible enthalpy, kJ/kg	U	velocity vector, m/s
h_0	enthalpy in reference state, kJ/kg	α	fin inclination, °
Δh	latent heat, kJ/kg	δ	fin thickness, mm
K	thermal conductivity of copper, W/(m·K)	ρ	density, kg/m^3
k_{c}	thermal conductivity of copper, W/(m·K)	v	kinematic viscosity, Pa·s
k_p	thermal conductivity of paraffin, W/(m·K)		

References

1. Rajvikram, M.; Rishi, P.; Muhammad, I.; Lucian, M.; Irfan, A.K.; Pietro, E. State-of-the-art sustainable approaches for deeper decarbonization in Europe—An endowment to climate neutral vision. *Renew. Sustain. Energy Rev.* **2022**, *159*, 112204.
2. Zhang, R.Y. *Phase Change Materials and Phase Change Energy Storage Technology*; Science Press: Beijing, China, 2009; pp. 1–127.
3. Rajvikram, M.; Leoponraj, S.; Ramkumar, S.; Akshaya, H.; Dheeraj, A. Experimental investigation on the abasement of operating temperature in solar photovoltaic panel using PCM and aluminium. *Sol. Energy* **2019**, *188*, 327–338.
4. Eslamnezhad, H.; Rahimi, A.B. Enhance heat transfer for phase-change materials in triplex tube heat exchanger with selected arrangements of fins. *Appl. Therm. Eng.* **2017**, *113*, 813–821. [CrossRef]
5. Darzi, A.A.R.; Jourabian, M.; Farhadi, M. Melting and solidification of PCM enhanced by radial conductive fins and nanoparticles in cylindrical annulus. *Energy Convers. Manag.* **2016**, *118*, 253–263. [CrossRef]
6. Ji, C.Z.; Qin, Z.; Low, Z.H.; Dubey, S.; Choo, F.H.; Duan, F. Non-uniform heat transfer suppression to enhance PCM melting by angled fins. *Appl. Therm. Eng.* **2018**, *129*, 269–279. [CrossRef]
7. Bhagat, K.; Prabhakar, M.; Saha, S.K. Estimation of thermal performance and design optimization of finned multitube latent heat thermal energy storage. *J. Energy Storage* **2018**, *19*, 135–144. [CrossRef]

8. Aly, K.A.; El-Lathy, K.R.; Fouad, M.A. Enhancement of solidification rate of latent heat thermal energy storage using corrugated fins. *J. Energy Storage* **2019**, *24*, 100785. [CrossRef]
9. Deng, S.X.; Nie, C.D.; Wei, G.Y.; Ye, W.B. Improving the melting performance of a horizontal shell-tube latent-heat thermal energy storage unit using local enhanced finned tube. *Energy Build.* **2019**, *183*, 161–173. [CrossRef]
10. Joshi, V.; Rathod, M.K. Constructal enhancement of thermal transport in latent heat storage systems assisted with fins. *Int. J. Therm. Sci.* **2019**, *145*, 105984. [CrossRef]
11. Joybari, M.M.; Haghighat, F.; Seddegh, S.; Al-Abidi, A.A. Heat transfer enhancement of phase change materials by fins under simultaneous charging and discharging. *Energy Convers. Manag.* **2017**, *152*, 136–156. [CrossRef]
12. Gürel, B. A numerical investigation of the melting heat transfer characteristics of phase change materials in different plate heat exchanger (latent heat thermal energy storage) systems. *Int. J. Heat Mass Transf.* **2020**, *148*, 119117. [CrossRef]
13. Song, X.N.; Ke, B.B.; Geng, Y.F.; Zhu, Q.Y. Numerical simulation of melting process for phase change material outside heating tube with fins. *J. Jiangsu Univ.* **2017**, *38*, 37–41.
14. Biwole, P.H.; Groulx, D.; Souayfane, F.; Chiu, T. Influence of fin size and distribution on solid-liquid phase change in a rectangular enclosure. *Int. J. Therm. Sci.* **2018**, *124*, 433–446. [CrossRef]
15. Bondareva, N.S.; Buonomo, B.; Manca, O.; Sheremet, M.A. Heat transfer inside cooling system based on phase change material with alumina nanoparticles. *Appl. Therm. Eng.* **2018**, *144*, 972–981. [CrossRef]
16. Bondareva, N.S.; Buonomo, B.; Manca, O.; Sheremet, M.A. Heat transfer performance of the finned nano-enhanced phase change material system under the inclination influence. *Int. J. Heat Mass Transf.* **2019**, *135*, 1063–1072. [CrossRef]
17. Masoumpour-Samakoush, M.; Miansari, M.; Ajarostaghi, S.S.M.; Arıcı, M. Impact of innovative fin combination of triangular and rectangular fins on melting process of phase change material in a cavity. *J. Energy Storage* **2022**, *45*, 103545. [CrossRef]
18. Kim, S.H.; Pandey, S.; Park, S.H.; Ha, M.Y. A numerical investigation of the effect of fin inclination angle on the thermal energy storage performance of a phase change material in a rectangular latent heat thermal energy storage unit. *J. Energy Storage* **2022**, *47*, 103957. [CrossRef]
19. Wu, J.T.; Chen, Q.C.; Zhang, Y.J.; Sun, K.L. Phase change material heat transfer enhancement in latent heat thermal energy storage unit with single fin: Comprehensive effect of position and length. *J. Energy Storage* **2021**, *42*, 103101. [CrossRef]
20. Mahood, H.B.; Mahdi, M.S.; Monjezi, A.A.; Khadom, A.A.; Campbell, A.N. Numerical investigation on the effect of fin design on the melting of phase change material in a horizontal shell and tube thermal energy storage. *J. Energy Storage* **2020**, *29*, 101331. [CrossRef]
21. Ghalambaz, M.; Chamkha, A.J.; Wen, D.S. Natural convective flow and heat transfer of Nano-Encapsulated Phase Change Materials (NEPCMs) in a cavity. *Int. J. Heat Mass Transf.* **2019**, *138*, 738–749. [CrossRef]
22. Singh, R.P.; Kaushik, S.C.; Rakshit, D. Melting phenomenon in a finned thermal storage system with graphene nano-plates for medium temperature applications. *Energy Convers. Manag.* **2018**, *163*, 86–99. [CrossRef]
23. Kamkari, B.; Shokouhmand, H. Experimental investigation of phase change material melting in rectangular enclosures with horizontal partial fins. *Int. J. Heat Mass Transf.* **2014**, *78*, 839–851. [CrossRef]
24. Kamkari, B.; Shokouhmand, H.; Bruno, F. Experimental investigation of the effect of inclination angle on convection-driven melting of phase change material in a rectangular enclosure. *Int. J. Heat Mass Transf.* **2014**, *72*, 186–200. [CrossRef]
25. Guo, Z.X.; Bai, Q.S.; Hou, J.L.; Yang, X.H.; Liu, Y.H.; Sun, Y.J. Experimental investigation on the melting behavior of phase change materials in open-cell metal foams in an inclined rectangular enclosure. *Energy Procedia* **2018**, *152*, 215–220. [CrossRef]
26. Zheng, H.P.; Wang, C.H.; Liu, Q.M.; Tian, Z.X.; Fan, X.B. Thermal performance of copper foam/paraffin composite phase change material. *Energy Convers. Manag.* **2018**, *157*, 372–381. [CrossRef]
27. Zhang, P.; Meng, Z.N.; Zhu, H.; Wang, Y.L.; Peng, S.P. Melting heat transfer characteristics of a composite phase change material fabricated by paraffin and metal foam. *Appl. Energy* **2017**, *185*, 1971–1983. [CrossRef]
28. Ghalambaz, M.; Zhang, J. Conjugate solid-liquid phase change heat transfer in heatsink filled with phase change material-metal foam. *Int. J. Heat Mass Transf.* **2020**, *146*, 118832. [CrossRef]
29. Yazici, M.Y.; Avci, M.; Aydin, O. Combined effects of inclination angle and fin number on thermal performance of a PCM-based heat sink. *Appl. Therm. Eng.* **2019**, *159*, 113956. [CrossRef]
30. Yagci, O.K.; Avci, M.; Aydin, O. Melting and solidification of PCM in a tube-in-shell unit: Effect of fin edge lengths' ratio. *J. Energy Storage* **2019**, *24*, 100802. [CrossRef]
31. Ghalambaz, M.; Hashem Zadeh, S.M.; Mehryan, S.A.M.; Pop, I.; Wen, D. Analysis of melting behavior of PCMs in a cavity subject to a non-uniform magneticfield using a moving grid technique. *Appl. Math. Model.* **2020**, *77*, 1936–1953. [CrossRef]
32. Sadegh, S.S.; Aghababaei, A.; Mohammadi, O.; Mosleh, H.J.; Shafii, M.B.; Ahmadi, M.H. An experimental investigation into the melting of phase change material using Fe_3O_4 magnetic nanoparticles under magnetic field. *J. Therm. Anal. Calorim.* **2021**, *146*, 381–392. [CrossRef]
33. Diao, Y.H.; Liang, L.; Zhao, Y.H.; Wang, Z.Y.; Bai, F.W. Numerical investigation of the thermal performance enhancement of latent heat thermal energy storage using longitudinal rectangular fins and flat micro-heat pipe arrays. *Appl. Energy* **2019**, *233–234*, 894–905. [CrossRef]
34. Bechiri, M.; Mansouri, K. Analytical study of heat generation effects on melting and solidification of nano-enhanced PCM inside a horizontal cylindrical enclosure. *Appl. Therm. Eng.* **2016**, *104*, 779–790. [CrossRef]

35. Ma, F.; Zhang, P.; Shi, X.J. Flow and heat transfer characteristics of micro-encapsulated phase change material slurry and energy transport evaluation. The 8th International Conference on Applied Energy–ICAE2016. *Energy Procedia* **2017**, *105*, 4607–4614. [CrossRef]

36. Zhao, J.D.; Zhai, J.; Lu, Y.H.; Liu, N. Theory and experiment of contact melting of phase change materials in a rectangular cavity at different tilt angles. *Int. J. Heat Mass Transf.* **2018**, *120*, 241–249. [CrossRef]

37. Feng, Y.C.; Li, H.X.; Li, L.X.; Bu, L.; Wang, T. Numerical investigation on the melting of nanoparticle-enhanced phase change materials (NEPCM) in a bottom-heated rectangular cavity using lattice Boltzmann method. *Int. J. Heat Mass Transf.* **2015**, *81*, 415–425. [CrossRef]

38. Gao, D.Y.; Tian, F.B.; Chen, Z.Q.; Zhang, D.L. An improved lattice Boltzmann method for solid-liquid phase change in porous media under local thermal non-equilibrium conditions. *Int. J. Heat Mass Transf.* **2017**, *110*, 58–62. [CrossRef]

39. Jourabian, M.; Farhadi, M.; Sedighi, K.; Darzi, A.R.; Vazifeshenas, Y. Simulation of natural convection melting in a cavity with fin using lattice Boltzmann method. *Int. J. Numer. Methods Fluids* **2010**, *70*, 313–325. [CrossRef]

40. Zhang, Y.D.; Zhang, X.L.; Ji, J.; Han, X.C. Progress in heat transfer enhancement of phase change materials. *J. Funct. Mater.* **2019**, *50*, 1056–1066.

41. Zhu, Z.Q. An Experimental Study of Melting Heat Transfer of Nanocomposite Phase Change Materials toward Thermal Energy Storage. Ph.D. Thesis, Zhejiang University, Hangzhou, China, 2018.

42. Jin, R.F. Experimental and Simulative Study on the Heat Storing Performance of the Solar Energy Storage with Phase Change Material. Master's Thesis, Donghua University, Shanghai, China, 2009.

43. Brent, A.D.; Voller, V.R.; Reid, K.J. Enthalpy-porosity technique for modeling convection-diffusion phase change: Application to the melting of a pure metal. *Numer. Heat Transf.* **1988**, *13*, 297–318. [CrossRef]

44. Ghalambaz, M.; Mehryan, S.A.M.; Mahdavi, M.; Younis, O.; Alim, M.A. Evaluation of the Melting Performance in a Conical Latent Heat Thermal Unit Having Variable Length Fins. *Sustainability* **2021**, *13*, 2667. [CrossRef]

45. Shmueli, H.; Ziskind, G.; Letan, R. Melting in a vertical cylindrical tube: Numerical investigation and comparison with experiments. *Int. J. Heat Mass Transf.* **2010**, *53*, 4082–4091. [CrossRef]

46. Asllanaj, F.; Parent, G.; Jeandel, G. Transient radiation and conduction heat transfer in a gray absorbing-emitting medium applied on two-dimensional complex-shaped domains. *Numer. Heat Transf. Part B Fundam.* **2007**, *52*, 179–200. [CrossRef]

47. Ghalambaz, M.; Mehryan, S.A.M.; Mozaffari, M.; Younis, O.; Ghosh, A. The Effect of Variable Length Fins and Different High Thermal Conductivity Nanoparticles in the Performance of the Energy Storage Unit Containing Bio-Based Phase Change Substance. *Sustainability* **2021**, *13*, 2884. [CrossRef]